J Solid State Electrochem (2011) 15:2447–2452
DOI 10.1007/s10008-011-1393-9

ORIGINAL PAPER

Comparison of transmissive permeable and reflective impermeable interfaces between electrode and electrolyte

Ju-Sik Kim · Su-Il Pyun

Received: 28 December 2010 / Revised: 1 April 2011 / Accepted: 2 April 2011 / Published online: 20 April 2011

Abstract This article described the basic concepts of the permeable boundary (PB) and impermeable boundary (IPB) conditions between electrode and electrolyte that are essential in studying diffusion and migration of ions through the electrode for electrochemical devices. The transmission line models (TLMs) were introduced to explain the boundary conditions at the electrode/electrolyte interfaces. The impedance data were simulated based upon the TLMs for PB and IPB conditions, giving attention to the different behaviors of low-frequency impedance. In addition, this article explained that the electrodes used for fuel cells and batteries can be classified according to the PB and IPB conditions.

Keywords Permeable boundary · Impermeable boundary · Transmission line model · Neutral atom diffusion · Ion migration · Warburg impedance

Introduction

In general, the hydrogen injection and evolution reaction, lithium intercalation and deintercalation reaction, and the oxygen reduction and hydrogen oxidation reaction are significantly affected by the transport of mobile ions through the electrodes for the electrochemical devices, such as electrochromic display devices, secondary batteries, and fuel cells [1–7]. Therefore, understanding ion diffusion (or migration) through the electrodes is of great importance to the elucidation of the overall reaction mechanism at the electrodes for the electrochemical systems.

There has been much interest in the numerical analyses of ion diffusion and migration through the electrodes in electrochemistry by using various electrochemical techniques, such as AC impedance spectroscopy [8–20], galvanostatic potential transient technique (chronopotentiometry) [14, 15], and potentiostatic current transient technique (chronoamperometry) [21–26]. For these electrochemical techniques, appropriate boundary conditions are necessary to obtain an analytical solution for ion transport. In particular, the behavior of ion transport for a relatively long time period is highly dependent on whether the boundary condition at the electrode and electrolyte interface is permeable or impermeable to mobile ions.

The boundary conditions at the interfaces have been described by theoretical impedance study in numerous articles [27–33]. The present work just gives a short review of the literature and book to show the concepts of two representative boundary conditions, permeable boundary (PB) and impermeable boundary (IPB), at the interfaces between electrode and electrolyte, by focusing on the discrepancy in low-frequency impedances for each boundary condition. In particular, the present work newly verifies that the impedance spectra simulated on simple model systems of fuel cell and secondary battery performances allow us to distinguish between PB and IPB constraints. We theoretically calculated the impedance spectra based upon the transmission line models (TLMs) under PB and IPB conditions and then discussed the boundary conditions commonly applied to the electrodes for fuel cells and battery, respectively.

Su-Il Pyun is an ISE member.

J.-S. Kim · S.-I. Pyun (✉)
Department of Materials Science and Engineering,
Korea Advanced Institute of Science and Technology,
373-1 Guseong-Dong, Yuseong-Gu,
Daejeon 305-701, Republic of Korea
e-mail: sipyun@kaist.ac.kr

Terminology of permeable (transmissive) boundary and impermeable (reflective) boundary

The boundary conditions for ion transport through an electrode can generally be divided into two categories: the permeable (transmissive) boundary (PB) and impermeable (reflective) boundary (IPB) conditions. Schematic diagrams of electrode geometry under these PB and IPB conditions are shown in Figs. 1 and 2, respectively, along with the indication of the direction of migration of ions and electrons and the corresponding Nyquist plots. Figure 1a shows the PB condition at the steady state of diffusion of neutral atoms or migration of ions under which atoms or ions enter into the entry side of the electrode via Faradaic reaction at the electrode/electrolyte interface on the left side, diffuse/migrate through the electrode, and escape from the exit side of the electrode. The injection (intercalation) into and extraction (deintercalation) of neutral atoms or ionic species from the specimen, i.e., the definite direction of their diffusion depends entirely upon whether either anodic or cathodic potential is externally applied to the input side of the specimen, but regardless of whether they are either neutral atoms or cations or anions. Thus, the electrode corresponding to the PB condition is also known alternatively as the symmetric electrode or free-standing membrane electrode.

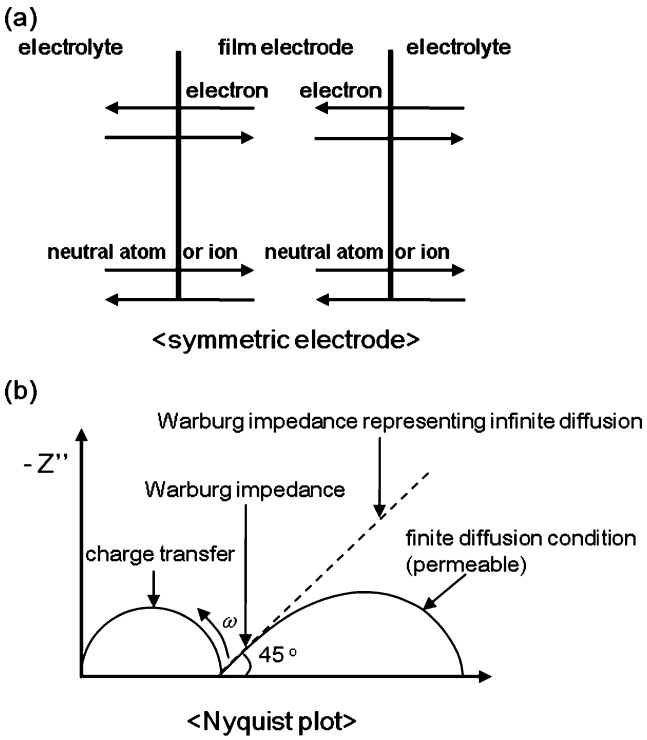

Fig. 1 **a** Schematic diagrams of symmetric electrode (electrode under permeable (transmissive) boundary (PB) condition) and **b** Nyquist plots of AC impedance PB condition

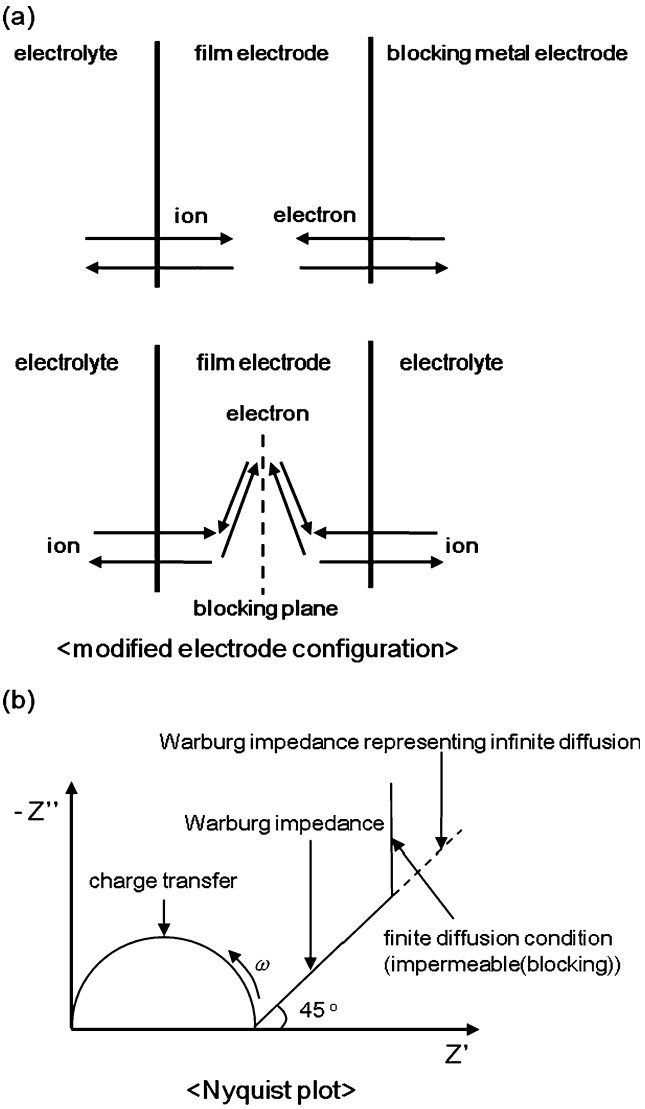

Fig. 2 **a** Schematic diagrams of modified electrode (electrode under impermeable (reflective) boundary (IPB) condition) and **b** Nyquist plot of AC impedance spectrum under IPB condition

In the Nyquist plot of Fig. 1b, the arc in the high-frequency range (on the left side) is associated with the interfacial reaction, which involves charge transfer at the electrode/electrolyte interface followed by ion penetration into the bulk electrode. Under this PB condition, the fluxes entering and leaving the electrode/electrolyte interfaces on each side become constant with time, i.e., they attain the steady state, and the electrode potential at the interface is determined by the value of ion flux. The straight line

inclined at a constant angle of 45° to the real axis (Warburg impedance) is attributed to the semi-infinite diffusion and migration of ion through the electrode. The slope of Warburg impedance deviates from 45° with decreasing frequency. This relates to ions moving out of the electrode into the electrolyte on the right side, resulting in the finite impedance. If the electrode thickness is infinite, Warburg impedance representing infinite diffusion would appear in the low-frequency range, as shown by the dotted line. The finite impedance is identical to the finite Warburg impedance, followed by a very small charge transfer resistance at low frequency. This just corresponds to the condition in which the electrode potential is determined at the PB interface (x = L) by the zero equilibrium concentration of ion.

Under the IPB condition at the local equilibrium established between ion and electron migrations as shown in Fig. 2a, ions are formed on the left side of the electrode from Faradaic reaction, followed by moving inside the electrode. In contrast to the PB condition, the mobile ions cannot penetrate through the back of the electrode but they accumulate at the metal/electrode interface. For instance, the direction of cationic flux for such as H^+ and Li^+, i.e., the injection (intercalation) into and extraction (deintercalation) from the specimen is always opposite to that direction of electronic flux because of the constraint of their local equilibrium, regardless of whether either anodic or cathodic potential is externally applied to the input side of the specimen. Therefore, the electrode corresponding to the IPB condition is also termed alternatively the modified electrode. The IPB condition can be also achieved by immersing the electrode into the electrolyte. In this case, ions are symmetrically injected into both sides of the electrode via Faradaic reactions and accumulate at the center of the electrode, which acts as the blocking plane against ion transport.

The AC impedance spectrum of Fig. 2b consists of an arc in high-frequency range, a straight line inclined at a constant angle of 45° to the real axis (Warburg impedance) in the intermediate-frequency range and a capacitive line (blocking region) in the low-frequency range. The arc represents the interfacial reaction for the ion injection, which involves charge transfer at the electrode/electrolyte interface on the left side (or both sides) of the electrode, and the Warburg impedance is related to the semi-infinite diffusion of ion in the electrode. The capacitive line in the Nyquist plot, which is vertical to the real axis (negative ∞ impedance), is related to the accumulation of ions at the blocking metal/electrode interface (or the center of the electrode). This is just identical to the condition in which the equilibrium electrode potential of electrode/electrolyte interface is determined, and the electrode potential is determined by the equilibrium ion concentration in electrodes with no concentration gradient.

The equilibrium electrode potential is the energy level of redox electron in the electrode rather than the electrostatic potential difference between electrode and electrolyte. We can easily realize such an equilibrium electrode potential with zero concentration of diffusing or migrating species at the PB interface and also that electrode potential with zero concentration gradient at the IPB interface.

Discussion and concluding remarks

The transmission line (TL) model is able to physically and mathematically express the two PB and IPB conditions for ion transport [34–41]. The TL model is conveniently used as a powerful tool to generate the PB and IPB conditions arbitrarily, depending upon whether the final circuit element of the original TL network is replaced by pure resistance or pure capacitance, respectively. Figure 3a, b shows the equivalent circuits of the TL networks, which represent the diffusion process in the electrode under the PB condition and IPB condition, respectively. Here, R_d (ohm per centimeter) designates the diffusion resistance per unit length, C_d (farad per centimeter) the chemical capacitance for diffusion per unit length, and x is the distance from the electrode/electrolyte interface towards PB and IPB. In TL model, the resistance of the charge transfer reaction at the electrolyte/electrode interface and the electronic resistance were assumed to be negligibly small compared to the diffusion resistance, thus disregarded. As the diffusing atoms move in the forward direction towards PB and IPB, they spatially and temporally sense instantaneous resistance to the movement as an R_d in the forward direction and simultaneously spatially and temporally do the instantaneous accumulation as a C_d downwards perpendicular to the forward direction. As a result, a "right-angle-shaped" R_dC_d series connection element is achieved.

The beginning boundaries of equivalent circuit bar (x=0) serve as electrolyte/electrode interfaces for the PB and IPB conditions. The only difference between the PB and IPB conditions is the capacitive element at the end of the equivalent circuit bar (x=L), which is replaced with the interfacial resistance R_{int} exposed to the electrolyte for the PB condition and the interfacial capacitance C_{int} adjacent to the electrode interior for the IPB condition.

For simplicity, let us assume that R_{int} and C_{int} are the same as R_d and C_d, respectively. Using Kirchhoff's voltage law on the circuits in Fig. 3a and b, the total finite diffusion impedance by Warburg circuit element Z_d (ohms) can be

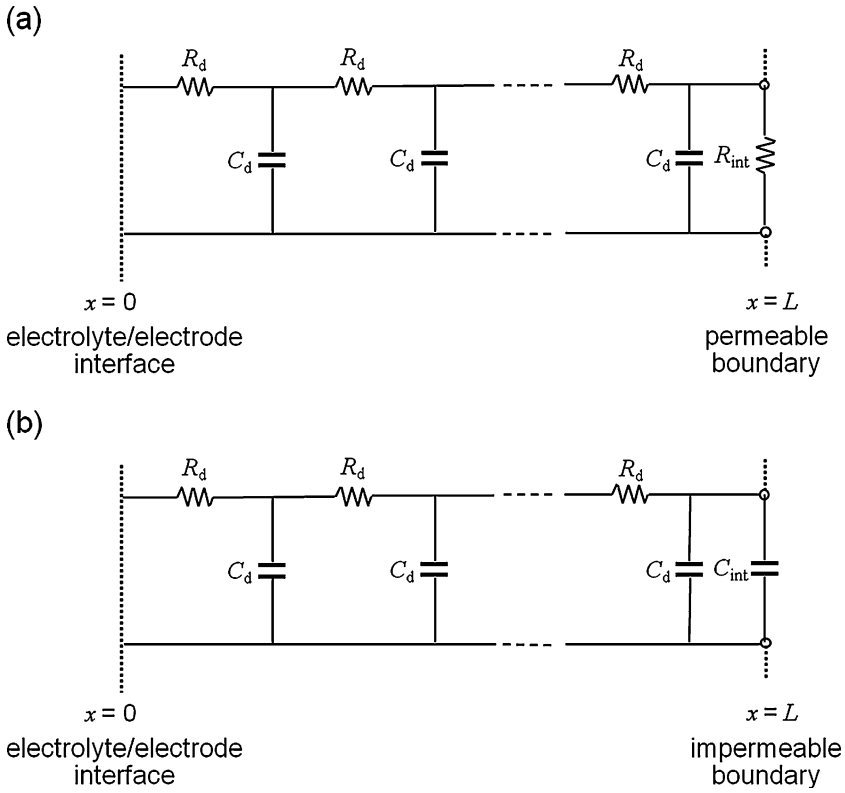

Fig. 3 Equivalent circuits of transmission line networks representing the diffusion process in the electrode under **a** permeable (transmissive) boundary (PB) condition and **b** one impermeable (reflective) boundary (IPB) condition

written in terms of R_d (ohm per centimeter) and C_d (farad per centimeter), depending upon the boundary conditions-under PB condition [6, 40],

$$Z_d(\omega) = R_d \frac{\tanh\left[L(j\omega R_d C_d)^{1/2}\right]}{(j\omega R_d C_d)^{1/2}} \quad (1)$$

under IPB condition [5, 41],

$$Z_d(\omega) = R_d \frac{\coth\left[L(j\omega R_d C_d)^{1/2}\right]}{(j\omega R_d C_d)^{1/2}} = R_d L \frac{\coth(j\omega/\omega_c)^{1/2}}{(j\omega/\omega_c)^{1/2}} \quad (2)$$

with $\omega_c = \frac{1}{R_d C_d L^2} = \frac{\widetilde{D}}{L^2}$ where L (centimeters) is the thickness (diffusion layer thickness) of the whole electrode, j [−] the unit of the complex number, i.e., $\sqrt{-1}$, $\sqrt{j} = \frac{1}{\sqrt{2}}(1+j)$), ω (hertz) the angular frequency, and ω_c (hertz) means the characteristic angular frequency of transition from a straight line inclined at 45° to the real axis (Warburg line) in the high-frequency range $\omega \gg \omega_c = \frac{\widetilde{D}}{L^2}$ to a capacitive line vertical to the real axis in the low frequency range $\omega \ll \omega_c = \frac{\widetilde{D}}{L^2}$ on the Nyquist plot. ω_c is conceptually equivalent to the reciprocal of the transition time t_{tr} in the potentiostatic current transient.

The Nyquist plots of the AC impedance spectrum calculated from Eqs. 1 and 2 are shown in Fig. 4a and b, respectively, by assuming L=1 cm, R_d=1 Ωcm^{-1}, and C_d= 0.01 $F cm^{-1}$. The characteristic difference in low-frequency impedance was found in Fig. 4a and b: the AC impedance spectrum exhibits the ideal Warburg behavior with an inclined phase angle of 45° at the high frequencies being the same as the case of IPB condition but a simple arc at the low frequencies being different from IPB condition. The transition frequency ω_c appears less markedly in transmissive PB condition than in reflective IPB condition. The AC impedance spectrum given in Fig. 4b depicts two characteristic features depending upon the frequency range, i.e., a straight Warburg line inclined at 45° to the real impedance axis in the high-frequency range above the characteristic(transition) frequency ω_c and the straight capacitive line with a phase angle of 90° vertical to the real axis in the low-frequency range below ω_c. The transition appears more sharply in reflective IPB condition than that in transmissive PB condition.

This discrepancy in the low-frequency impedance between the PB and IPB conditions results from the different end elements of the equivalent circuit bar, either resistance or capacitance. Therefore, the impedance behavior at low frequencies highly depends upon whether the mobile ions are either passing through the electrolyte/electrode interface permeable to themselves or accumulated at IPB impermeable to themselves.

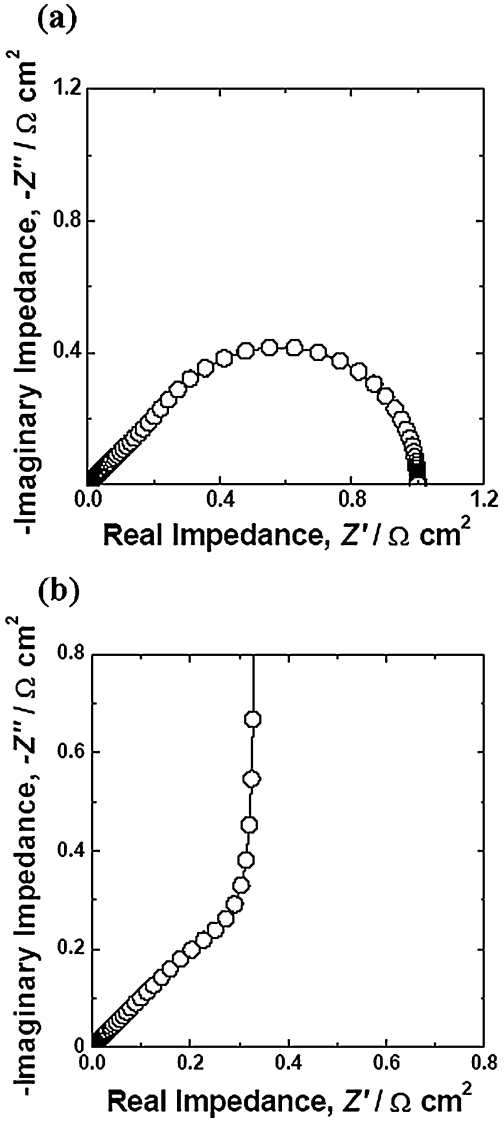

Fig. 4 Nyquist plot of the AC impedance spectrum theoretically calculated for diffusion in the planar electrode in **a** the permeable (transmissive) boundary(PB) condition from Eq. 1 and **b** the impermeable (reflective) boundary(IPB) condition from Eq. 2

In practice, the electrodes for fuel cells are often viewed as the symmetric electrode corresponding to the PB condition. In solid oxide fuel cells (SOFCs), for example, oxygen ions are generated by the cathodic reaction and delivered to the electrolyte [42, 43]. At the anode, the oxygen ions are consumed by fuel at the electrolyte interface, producing combustion products and electrons [43, 44]. During the overall electrochemical processes for fuel cells, there is no accumulation of charged particles inside the electrodes, and the electrodes can be regarded as the symmetric electrode. Like SOFCs, the PB condition is adopted for the analyses of impedance spectra and current transients obtained from the electrodes for polymer electrolyte membrane fuel cells (PEMFCs) [45, 46]. In fact, the low-frequency arc representing the permeable condition for TLM in Fig. 4a was found to be in good agreement with the impedance spectra experimentally measured from the electrodes for SOFC and PEMFC [7, 42, 45, 46]. For the permeable electrode, the current at the steady-state condition provides useful information in analyzing the kinetics of electrode reactions. For instance, the variation in the steady-state current observed for the potentiostatic current transients allows us to elucidate the mechanism changes of electrode reaction during the operating conditions [6, 7, 42].

The electrode geometry satisfying the IPB condition is adopted in the electrochemical devices, such as lithium ion and Ni/metal hydride secondary batteries [47, 48]. For normal batteries, mobile ions are usually accumulated at the electrodes. For example, the interface between the lithium vanadium ($Li_\delta V_2O_5$) oxide film and metal substrate is impermeable to lithium ions because of the low solubility of lithium in vanadium [47, 48]. Intercalated lithium ions accumulate at the oxide/metal interfaces after three consecutive steps of charge transfer at the electrode/electrolyte interface, and the ions are absorbed into the oxide film and diffused through the oxide film. In the case of the hydrogen absorption reaction and the hydrogen evolution reaction from Pd foil electrode, the center of the Pd electrode is also considered as a blocking plane for hydrogen diffusion [11–13]. As a matter of fact, the capacitive line at low frequencies shown in Fig. 4b was observed to be in good agreement with real electrodes for secondary batteries and metal–hydrogen systems [12, 41, 48]. Under the IPB conditions, the currents or potentials at the electrodes are close to the equilibrium values, so that the chemical and component diffusivity of mobile ions can be evaluated from the analyses of AC impedance spectra and galvanostatic intermittent titration curve [12, 47].

In summary, it is concluded that the difference between the symmetric electrode and the modified electrode, the two types of electrodes used for studying migration of ions through the electrode, is well understood as analogous to that difference in the electrode/electrolyte interface between pure resistive and pure capacitive elements at the end of the original TL network. The electrodes for batteries and fuel cells are also classified into two types according to the boundary conditions. The PB condition is usually readily applied to the electrode of fuel cells, while the IPB condition is conveniently adopted for the electrode of batteries. Thorough understanding of the concept of the PB and IPB conditions is important in studying ion transports through electrodes for the electrochemical devices.

Simulation procedure

The simulations of AC impedance spectra were performed by a commercial MathCad software (MathSoft

Inc., Cambridge, MA). The overall impedances were calculated in the frequency range between 10^{-2} and 10^{5} Hz based upon the analytical solutions describing each transmission line circuit in Fig. 3a and b.

References

1. Fuller TF, Newman J (1995) In: White RE, Bockris JO'M, Conway BE (eds) Modern aspects of electrochemistry. vol. 27. Plenum, New York, p 359
2. Gu WB, Wang CY, Li SM, Geng MM, Liaw BY (1999) Electrochim Acta 44:4525–4541
3. Feng F, Geng M, Northwood DO (2001) Int J Hydrogen Energy 26:725–734
4. Wronski ZS (2001) Int Mater Rev 46:1–49
5. Lee JW, Pyun SI (2005) Electochim Acta 50:1777–1805
6. Kim JS, Pyun SI (2008) Isr J Chem 48:277–286
7. Kim JS, Pyun SI, Shin HC, Kang SJL (2008) J Electrochem Soc 155:B762–B769
8. Lim C, Pyun SI (1993) Electrochim Acta 38:2645–2652
9. Lim C, Pyun SI (1994) Electrochim Acta 39:363–373
10. Zhang W, Sridhar Kumar MP, Srinivasan S, Ploehn HJ (1995) J Electrochem Soc 142:2935–2943
11. Yang TH, Pyun SI (1996) Electrochim Acta 41:843–848
12. Yang TH, Pyun SI (1996) J Electroanal Chem 414:127–133
13. Yang TH, Pyun SI (1996) J Power Sources 62:175–178
14. Feng F, Ping X, Zhou Z, Geng M, Han J, Northwood DO (1998) Int J Hydrogen Energy 23:599–602
15. Haran BS, Popov BN, White RE (1998) J Electrochem Soc 145:4082–4090
16. Wang C (1998) J Electrochem Soc 145:1801–1812
17. Montella C (1999) J Electroanal Chem 462:73–87
18. Montella C (2000) J Electroanal Chem 480:166–185
19. Yuan X, Xu N (2002) J Electrochem Soc 149:A407–A413
20. Georen P, Hjelm AK, Lindbergh G, Lundqvist A (2003) J Electrochem Soc 150:A234–A241
21. Conway BE, Wojtowicz J (1992) J Electroanal Chem 326:277–297
22. Ura H, Nishina H, Uchida I (1995) J Electroanal Chem 396:169–173
23. Nishina T, Ura H, Uchida I (1997) J Electrochem Soc 144:1273–1277
24. Kim HS, Nishizawa M, Uchida I (1999) Electrochim Acta 45:483–488
25. Feng F, Han J, Geng M, Northwood DO (2000) J Electroanal Chem 487:111–119
26. Yuan X, Xu N (2001) J Appl Electrochem 31:1033–1039
27. Diard JP, Gorrec BL, Montella C (1999) J Electroanal Chem 471:126–131
28. Lasia A (1999) Mod Aspects Electrochem 32:143–248
29. Montella C (2000) J Electroanal Chem 480:150–165
30. Montella C (2001) J Electroanal Chem 497:3–17
31. Lasia A (2002) Mod Aspects Electrochem 35:1–49
32. Diard JP, Glandut N, Montella C, Sanchez JY (2005) J Electroanal Chem 578:247–257
33. Bard AJ, Inzelt G, Scholz F (eds) (2008) Electrochemical dictionary. Springer, Berlin, p. 347
34. Raistrick ID (1990) Electrochim Acta 35:1579–1586
35. Bisquert J, Garcia-Belmonte G, Bueno P, Longo E, Bulhoes LOS (1998) J Electroanal Chem 452:229–234
36. Bisquert J, Compte A (2001) J Electroanal Chem 499:112–120
37. Jamnik J, Maier J (2001) Phys Chem Chem Phys 3:1668–1678
38. Bisquert J (2002) Electrochim Acta 47:2435–2449
39. Boukamp BA (2004) Solid State Ionics 169:65–73
40. Barsoukov E, Macdonald JR (2005) Impedance spectroscopy. Wiley, New York, p. 16, p. 54
41. Lee JW, Pyun SI (2005) Z Metallkd 96:117–123
42. Kim JS, Pyun SI (2009) Electrochim Acta 54:952–960
43. Vohs JM, Gorte RJ (2009) Adv Mater 21:943–956
44. Gorte RJ, Vohs JM (2009) Curr Opin Colloid In 14:236–244
45. Lee SJ, Pyun SI (2007) Electrochim Acta 52:6525–6533
46. Lee SJ, Pyun SI (2008) J Electrochem Soc 155:B1274–B1280
47. Bae JS, Pyun SI (1995) J Alloys Compd 217:52–58
48. Pyun SI, Bae JS (1996) Electrochim Acta 41:919–925